TEMPORAL FILTERS FOR ISOLATING STEADY PHOTOSPHERIC FLOWS

DAVID H. HATHAWAY

Space Science Laboratory, NASA Marshall Space Flight Center, Huntsville, AL 35812, U.S.A.

(Received 5 April, 1988)

Abstract. A variety of temporal filters are tested on artificial data with 60 and 75 s sampling intervals to determine their accuracy in separating the nearly-steady photospheric flows from the p-mode oscillations in Doppler velocity data. Longer temporal averages are better at reducing the residual signal due to p-modes but they introduce additional errors from the rotation of the supergranule pattern across the solar disk. Unweighted filters (boxcar averages) leave residual r.m.s. errors of about 6 m s^{-1} from the p-modes after 60 min of averaging. Weighted filters, with nearly Gaussian shapes, leave similar residual errors after only 20 min of averaging and introduce smaller errors from the rotation of the supergranule pattern. The best filters found are weighted filters that use data separated by 150 or 120 s so that the p-modes are sampled at opposite phases. These filters achieve an optimum error level after about 20 min, with the r.m.s. errors due to the p-mode oscillations and the rotation of the supergranules both at a level of only 1.5 m s^{-1}.

1. Introduction

Measurements of solar velocity fields from the Doppler shifts of photospheric spectral lines include contributions from a variety of velocity components. Accurate analyses of these components usually require separating them so that the contributions from the other components are minimized. Temporal filters must be used to separate the 5 min oscillations, or p-modes, from the nearly flows such as rotation, differential rotation, meridional circulation, and supergranulation. One such filter, used by Leighton, Noyes, and Simon (1962) for studying supergranulation, takes a simple average of two observations separated by about 150 s to reduce the signal due to the p-modes. With the advent of helioseismology, long strings of Doppler velocity images are now available for the study of the p-modes. These strings are also ideal for studies of the nearly steady flows and allow the use of more sophisticated temporal filters for removing the p-mode oscillations. Long temporal averages have been suggested for these filters. However, the length of the average must not become too long or the rotation and evolution of the supergranulation pattern will introduce errors in the filtered velocity image.

In this paper a variety of temporal filters are tested to determine their efficiency in reducing the signal due to the p-mode oscillations while keeping the errors due to the rotation of the supergranule pattern at a minimum. Artificial data are used for testing the filters. Two time strings, with data points separated by 75 and 60 s, are constructed to represent the signal due to the p-mode oscillations. A series of two-dimensional Doppler velocity images with different central meridians are constructed to represent the rotation of the nearly steady-flow pattern. These artificial data sets are described in the following section. The filters themselves, and their response to the p-mode oscillations, are described in Section 3. In Section 4, an analysis of the errors induced

Solar Physics **117** (1988) 1–12.

by the rotation of the supergranule pattern is used to identify the optimum filter. Although a limited variety of filters are examined in this paper, they represent broad classes of filter types. The one filter found to be most effective for reducing the residual velocity errors has unique characteristics which are tailored for the problem at hand.

2. Artificial Data for Testing the Temporal Filters

Although the shape of a filter in frequency space indicates its effectiveness in suppressing certain frequencies, artificial data play a key role in actually testing the various filters and quantifying the results. Time series containing only p-mode oscillations or only the rotation of the steady flow pattern are used separately to determine the response of the different filters to these phenomena. Care must be taken to insure that the data are realistic and faithfully represent the solar velocity fields they portray. Absolute realism is, of course, impossible, but realistic data with the important attributes of the actual data can be constructed.

Two time series are constructed to represent Doppler measurements of the p-mode oscillations. One time series has the 75 s sampling interval chosen for the Global Oscillation Network Group (GONG) project; the other has the 60 s interval that is often used for observations of the p-modes. Both time series represent the response of a spatial filter (arbitrarily taken to be the spherical harmonic with degree $l = 42$ and order $m = 21$) to a string of Doppler images. Since only one hemisphere is seen in a Doppler image, this spatial filter is susceptible to crosstalk from other spherical harmonic modes. The contributions to the power spectrum from these adjacent modes are given in Table I, where contributions smaller than 0.0001 are represented by dashes.

TABLE I

Contributions to the power spectrum from adjacent modes

$m\backslash l$	38	39	40	41	42	43	44	45	46
17	0.0012	–	0.0024	–	0.0003	–	–	–	–
18	–	–	–	–	–	–	–	–	–
19	0.0022	–	0.0820	–	0.0275	–	0.0003	–	–
20	–	–	–	0.5673	–	0.0684	–	–	–
21	0.0001	–	0.0240	–	0.9577	–	0.0262	–	0.0002
22	–	–	–	0.0595	–	0.5625	–	–	–
23	–	–	0.0001	–	0.0230	–	0.0866	–	0.0022
24	–	–	–	–	–	–	–	–	–
25	–	–	–	–	0.0001	–	0.0023	–	0.0018

The time series are constructed by making a power spectrum for the p-modes, choosing random phases at each frequency point, and then taking the Fourier transform of the complex amplitude spectrum. The power spectrum is constructed by taking each of the contributing spherical harmonics and finding the frequency for each mode using

(adapted from Harvey and Duvall, 1984)

$$\nu(n, l) = 2354.2(n + 1.57)\exp[0.2053[[(\ln x - 14.523)^2 + 4.1175]^{1/2} - \ln x]]\ \mu\text{Hz} \quad (1)$$

with

$$x = (n + 1.57)\pi R_\odot [l(l + 1)]^{-1/2}, \quad (2)$$

where n is the radial wavenumber and $R_\odot$ is the solar radius in km. This expression gives frequencies which closely match the observed mode frequencies given by Duvall *et al.* (1988) with differences of about 1 μHz at the lowest frequencies and about 10 μHz at the highest frequencies. A rotational splitting term corresponding to a rigid rotation of the Sun is also included with $\Delta\nu = 0.444m$, where m is the azimuthal order of the mode.

The power at each mode frequency is given by the product of the relative contribution given in Table I and an envelope function (Leibacher, 1987)

$$P(\nu) = 0.5[1 + 0.00075(\nu - 2750)]^2 \exp[(\nu - 2750)^2/750^2], \quad \nu > 1427\ \mu\text{Hz}, \quad (3)$$

which is an approximation to the data of Grec, Fossat, and Pomerantz (1983). Each peak in the power spectrum is given a Lorentzian line shape with a FWHM that

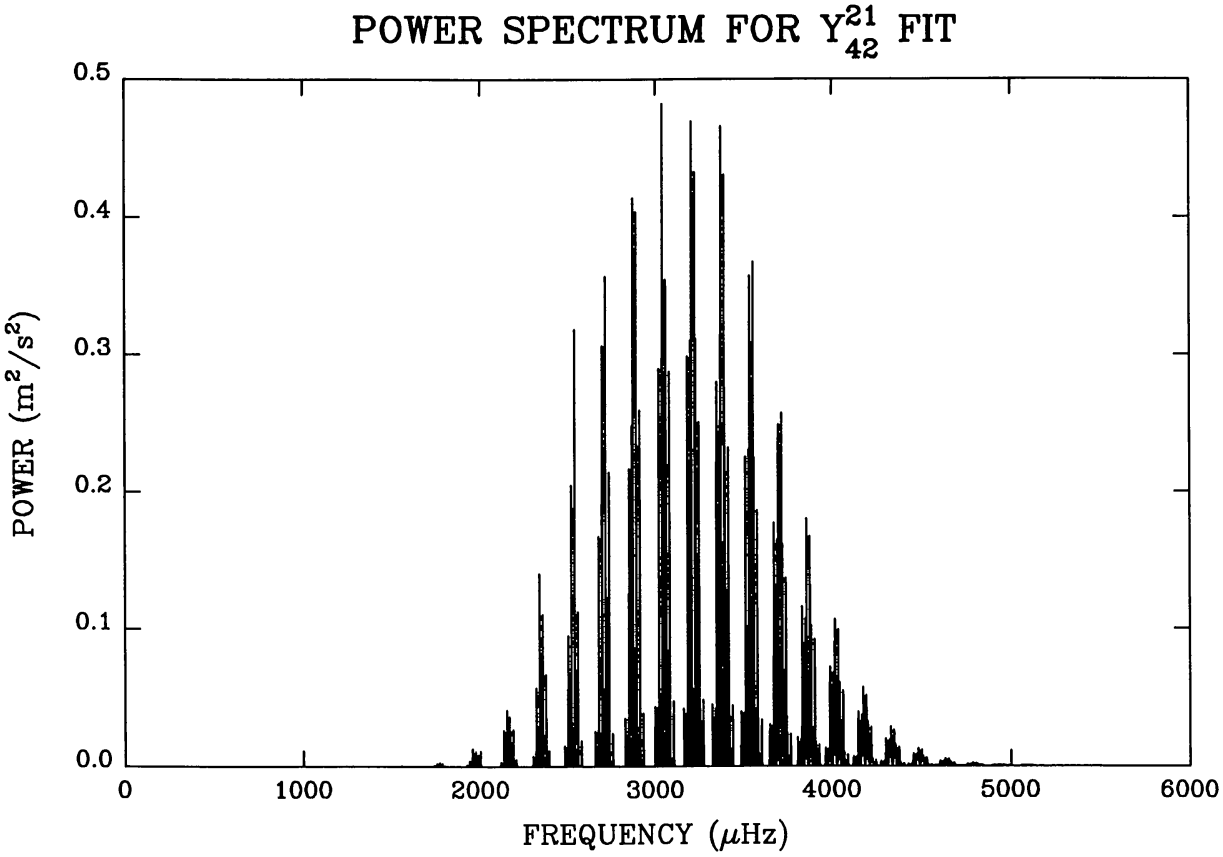

Fig. 1. Power spectrum for the p-mode oscillation time series. The full spectrum extends to 13 333 μHz for the 75 s series and to 16 667 μHz for the 60 s series with 0.1 μHz samples. The spikes are Lorentzian line profiles at the frequencies of the modes that contribute to the Y_{42}^{21} spatial filter. Only those modes with frequencies between about 1500 μHz and about 5500 μHz contribute to the oscillations.

approximates the results of Libbrecht and Zirin (1986). The line widths increase smoothly from 0.5 μHz at the lowest frequencies to 1.5 at 3000 μHz to 4.5 at 4000 μHz. The resulting power spectrum is shown in Figure 1. This spectrum compares favorably with those shown by Grec, Fossat, and Pomerantz (1983) and Libbrecht and Zirin (1986) and includes several important characteristics. The envelope of the spectrum closely matches the observed envelope and includes substantial power from about 2000 μHz up to about 5000 μHz. It includes a rich array of spectral peaks that closely matches the measured frequencies and lifetimes for the modes.

The power spectrum was evaluated from $\nu = 0$ to $\nu = 13\,333$ μHz for the 75 s sampling rate and to $\nu = 16\,667$ μHz for the 60 s sampling rate. The spectrum was sampled at 0.1 μHz intervals. This gives a repeat time for the time series of about 116 days. The first 4 hours of the 75 s time series are shown in Figure 2. This time series exhibits several important characteristics of the p-mode oscillations. The series shows variations with periods near 5 min and an apparent coherence time of about 20 min due to the width of the p-mode frequency band given by Equation (3).

Two-dimension images of the Doppler velocity fields are produced using the method described by Hathaway (1988). The velocity fields are represented by a spectrum of

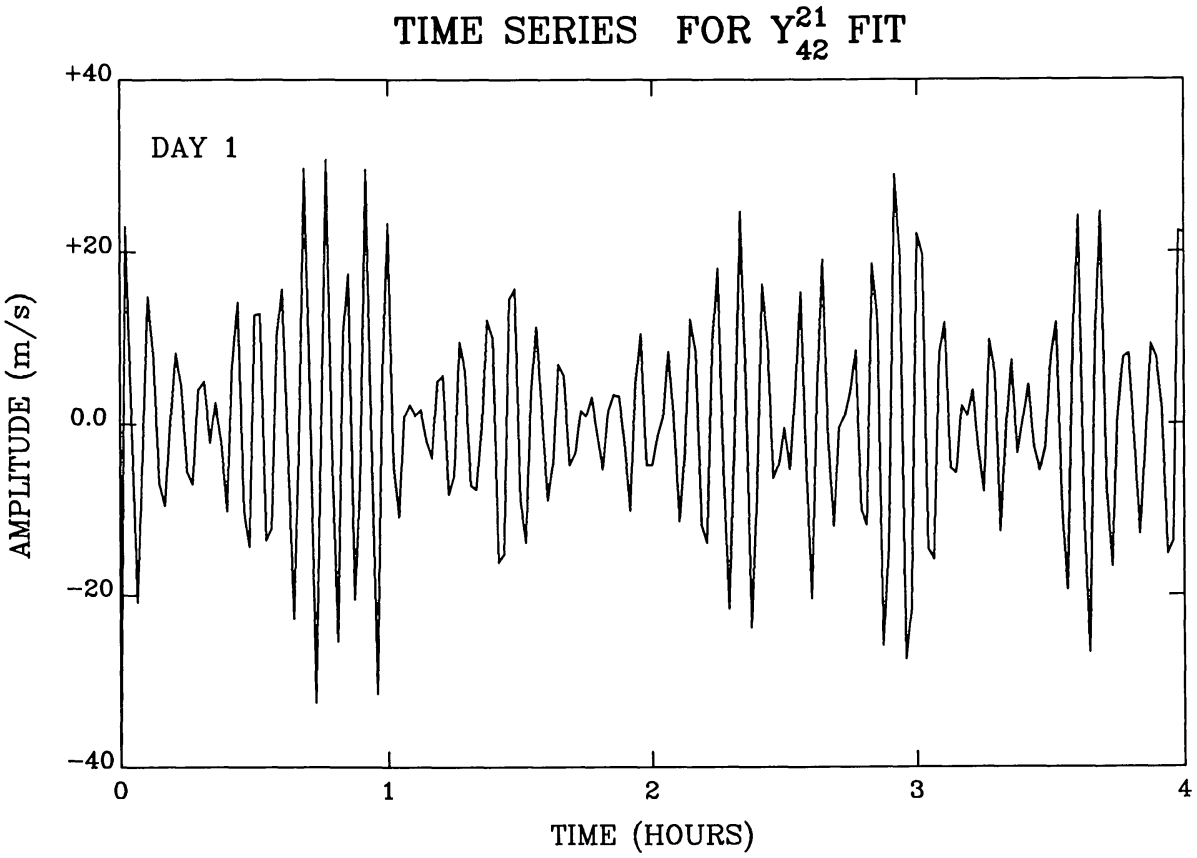

Fig. 2. The first 4 hours of the 75 s sample time series. The full time series continues for about 116 days before repeating and retains the same characteristics throughout. The oscillations are quasi-periodic with periods of about 5 min and appear coherent for only about 20 min because of interference with other modes with similar periods.

spherical-harmonic modes which determines the vector velocity field in the solar photosphere. These vector velocity components are projected into the line-of-sight to give the Doppler velocity at every pixel on the solar disk in a 256 by 256 pixel image. To test the response of the filters to the rotation of the supergranulation pattern, images containing only the steady flow components (rotation, differential rotation, meridional circulation, supergranulation, limb shift, and giant cells) are made. The central longitude of each image is shifted to represent the time of the observation. This gives a rigid rotation of the supergranulation pattern through 0.55° in 1 hour. (Differential rotation of the supergranulation should play a minor role over this time interval and is neglected.) This angular displacement is large enough to move the pattern through about a quarter of a supergranule at the equator and introduces differences in the observed velocity at a given pixel of nearly 500 m s^{-1}. The supergranule pattern and the difference between two images taken 1 hour apart are shown in Figure 3.

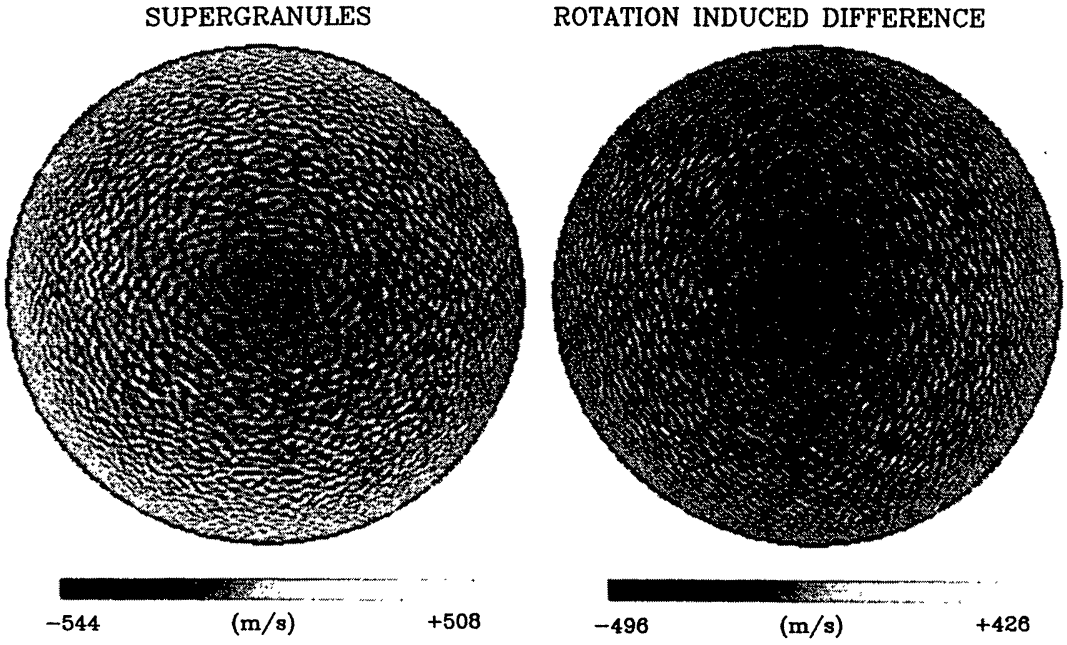

Fig. 3. Doppler velocity images for the supergranules and the rotation induced difference between two steady flow images separated by 60 min. Dark areas are approaching the observer; light areas are receding. The supergranulation image illustrates the realism of the data. The convection cells have the size, velocity amplitude, and randomness of real supergranules. The second image illustrates the magnitude and nature of the differences between two Doppler images separated by 1 hour. It indicates the need for short temporal averages.

3. Residual Errors Due to the *p*-Mode Oscillations

The artificial time series can be used to test the response of various filters by running the filters across the data to get a running mean and then comparing the amplitude of this filtered time series to the amplitude of the original. Three different types of filters

are constructed for this exercise and the length of each filter type is varied to determine its characteristics.

The first filter type is the 'boxcar' filter. This filter uses equal weights for all points in time over the length of the filter and is represented in the time domain by

$$F_B^k[V(t)] = \sum_{j=0}^{k} \left[\frac{1}{k+1}\right] V(t_0 + j\Delta t)\,, \tag{4}$$

where Δt is the sampling interval and $V(t)$ represents the velocity data at time t. Assuming a continuous average with no gaps, the shape of this filter in the frequency domain is given by

$$\tilde{F}_B^k[\tilde{V}(\nu)] = \left[\frac{\sin 2\pi\nu k\Delta t}{2\pi\nu k\Delta t}\right] \tilde{V}(\nu)\,, \tag{5}$$

where the tildes indicate the Fourier transformed quantities and $k\Delta t$ is the full length of the filter.

Another filter type assigns unequal weights to each point and is called a 'weighted' filter throughout this paper. This particular weighted filter is generated by a basic filter given by the average of two measurements. This basic filter is used to produce a filtered time string which can be filtered again in the same manner. When applied k times, the resulting filter is given by

$$F_W^k[V(t)] = \sum_{j=0}^{k} \left[\frac{1}{2^k} \frac{k!}{j!\,(k-j)!}\right] V(t_0 + j\Delta t) \tag{6}$$

in the time domain, where the factorial terms are just the binomial coefficients given by Pascal's triangle. For large k this filter is nearly Gaussian in shape in the time domain. In the frequency domain this filter is given by

$$\tilde{F}_W^k[\tilde{V}(\nu)] = [\tfrac{1}{2} + \tfrac{1}{2}\cos 2\pi\nu\Delta t]^k\, \tilde{V}(\nu) \tag{7}$$

which gives narrow peaks in the transmission of the filter at frequencies $\nu = 0$ and $\nu = 1/\Delta t$. As defined here this weighted filter uses the sampling interval, 75 or 60 s, for Δt.

The third filter type is closely related to the weighted filter in that it uses the same weights but takes $\Delta t = 150$ s for the 75 s series and $\Delta t = 120$ s for the 60 s series. Since it uses every other point in time it is called a 'weighted comb' filter throughout this paper. Note that for $k = 1$ the weighted comb filter becomes the same filter used by Leighton, Noyes, and Simon (1962) and by many others since. The advantage of the weighted comb filter is that it samples the modes with 5 or 4 min periods at opposite phases of oscillation and thus greatly reduces their transmitted power.

The characteristic shape of these three filters is shown in Figure 4 in both the time domain, upper row, and the frequency domain, bottom row. The dotted line in each of the frequency domain plots represents the envelope of the power spectrum for the

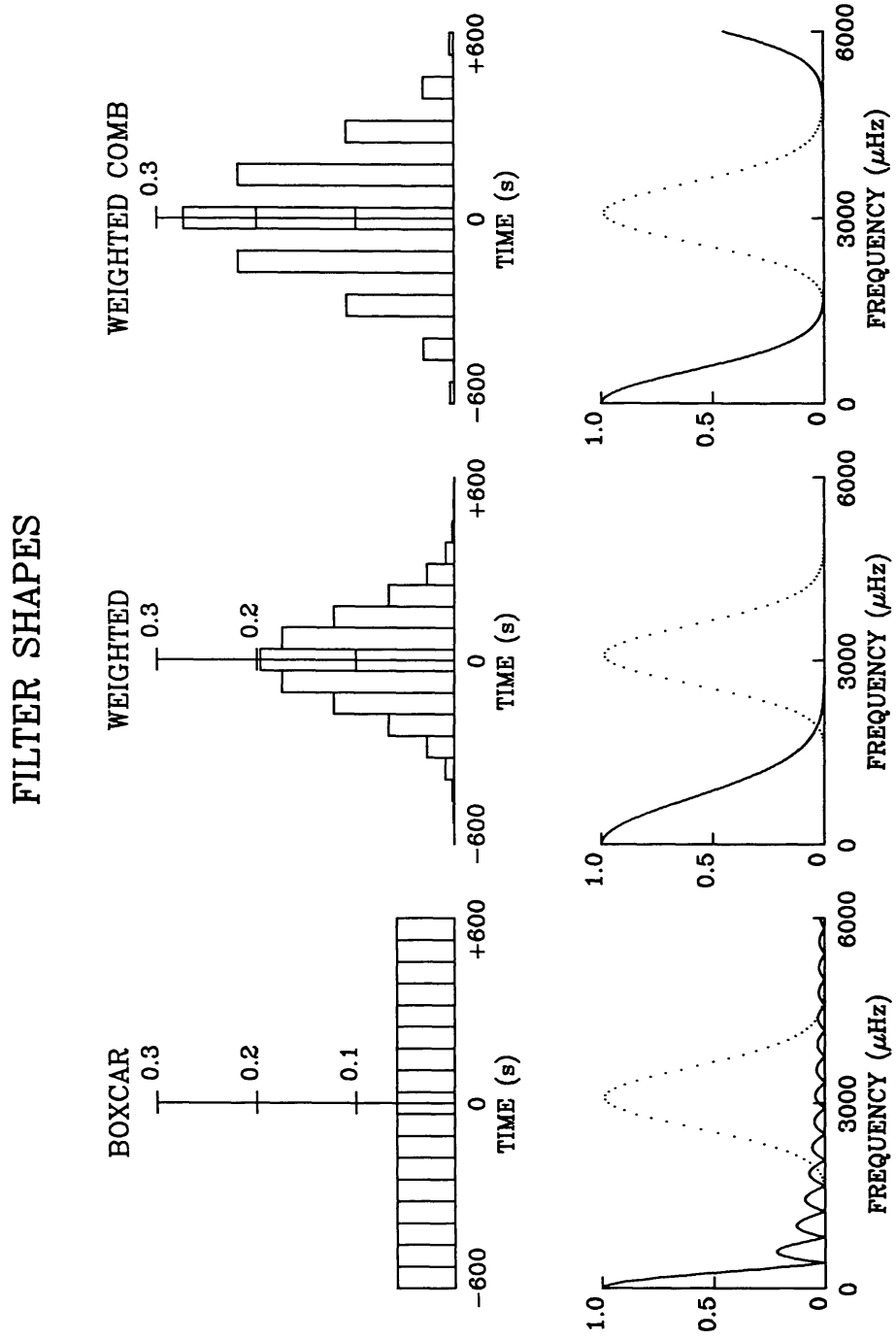

Fig. 4. The shapes of the three different filter types are shown in the time domain along the top row and in the frequency domain along the bottom row. The dotted line in each of the frequency domain plots shows the envelope of the power spectrum for the p-modes. The boxcar filter has several small transmission peaks across this envelope. The weighted filter has only a small overlap with the p-mode frequencies and the weighted comb filter excludes nearly the entire p-mode band.

p-modes as given by Equation (3). The temporal length of each filter shown in Figure 4 is taken to be 20 min and the sampling interval was taken to be 75 s. While the descriptive names for the filters are suggested by the shapes of the filters in the time domain, the relative effectiveness of each filter type in suppressing the p-mode velocity signal can be estimated from their shape in the frequency domain. The boxcar filter has several small peaks in transmission throughout the range of p-mode frequencies. The weighted filter has a small overlap at the low-frequency end of the p-mode range. The weighted comb filter should be the most effective at suppressing the p-modes, since, for the 20 min filter length ($k = 8$), it has virtually no transmission at all the p-mode frequencies.

This cursory assessment of the response of these filters can be tested by running them across the artificial time series and comparing the transmitted signal to the original. The results of this test are shown in Figure 5 for the filtering of the 75 s series by each filter type. The r.m.s. amplitude of the filtered signal is plotted vertically as a percentage of the r.m.s. amplitude of the original signal. The full temporal length of each filter is indicated by its position along the horizontal axis. The response of the boxcar filters is shown by the solid line, the response of the weighted filters is represented by the filled

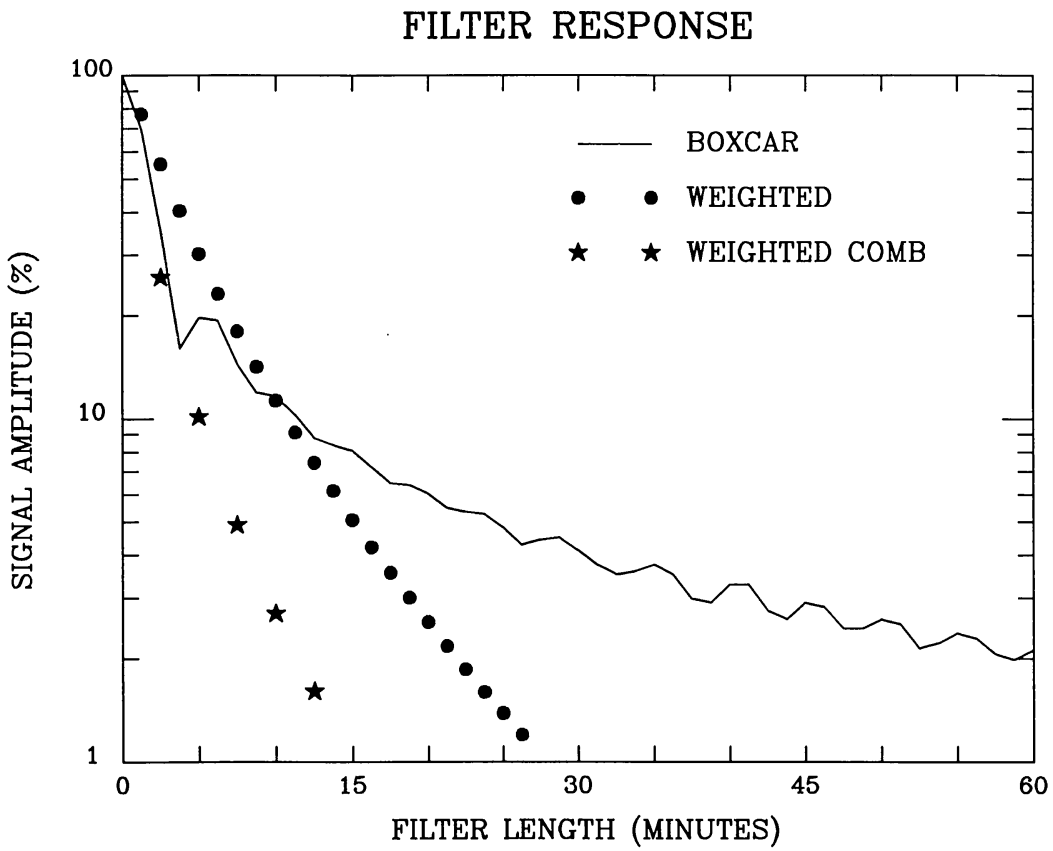

Fig. 5. The response of each of the three different filter types is represented by the residual signal amplitude as a function of filter length. A 60 min boxcar filter still transmits about 2% of the p-mode signal. A weighted filter achieves the same level of performance in about 20 min while a weighted comb filter requires a length of only 10 min.

circles, and the response of the weighted comb filters is given by the stars. This test supports and quantifies the assessment of the filters from their shape in the frequency domain. The boxcar filter still passes about 2% of the signal when the filter is 60 min long. If 300 m s^{-1} is a typical r.m.s. amplitude for the p-mode signal, then this gives a residual signal from the 60 min boxcar filter of about 6 m s^{-1}. The weighted filter becomes this effective after about 20 min while the weighted comb filter requires only about 10 min to achieve this level of performance.

Similar results are obtained with the 60 s series. As expected, the boxcar filter gives virtually identical results with both time series. However, the weighted and weighted comb filters exhibit some differences. For the 60 s series the weighted filters are less effective for a given filter length than those used on the 75 s series. For weighted filters with a full width of 10 min and longer, the 60 s sampling rate is nearly half as effective as the 75 s sampling rate. The reason for this difference is to be found in the shape of the filters in the frequency domain. The 75 s sampling rate gives transmission peaks at $\nu = 0$ and $\nu = 13\,333$ μHz with no transmission at $\nu = 6667$ μHz. The 60 s sampling rate gives transmission peaks at $\nu = 0$ and $\nu = 16\,667$ μHz and no transmission at $\nu = 8333$ μHz. This gives a larger overlap with the p-mode frequency band for the 60 s series filters so that more p-mode signal is passed by these filters. For the weighted comb filters, the comparison with the 75 s series shows a more mixed response. The 75 s series filters are somewhat more effective for filter lengths shorter than about 20 min while the 60 s series filters are better for the longer filter lengths. In fact, the weighted comb filters for the 60 s series are nearly twice as effective as those for the 75 s series when the filter length reaches 30 min.

4. Residual Errors Due to the Rotation of the Supergranules

The results of the preceding section indicate that the weighted comb filters are the most efficient at filtering out the p-mode oscillation signal. While the velocity errors that are passed by these filters become smaller quite rapidly as the filter length increases, the longer filters will introduce new errors in the velocity signal due to the rotation of the supergranule pattern. This problem might be circumvented by mapping the velocity images onto a rotating heliocentric coordinate system. However, this introduces additional problems associated with determining consequential changes in the line-of-sight velocity and using the proper rotation rate at each latitude. In addition there is the obvious problem of the additional computational work that must be implemented in this scenario. Before proceeding in this direction it must be determined how severe the problem actually is. The rotation-induced velocity difference shown in Figure 3 represents an extreme case in which two images separated by 60 min are compared. In this section the weighted comb filters themselves are applied to a series of artificial Doppler velocity images to determine the magnitude of the errors introduced by the rotation of the supergranule pattern.

A series of 13 two-dimensional Doppler velocity images are constructed using the method described by Hathaway (1988). The same supergranule pattern was used in each

image but the central meridians were displaced by 0.0229° between each successive image. This series represents the rotation of the Sun over 30 min using images separated by 150 s. Filtered images are constructed by taking weighted averages of the images in the series where the weights are prescribed by the term in brackets in Equation (6). The differences between these filtered images and the individual images corresponding to the central time of the filters give a quantitative measure of the errors introduced by the rotation of the Sun. For the even numbered filters, the central image is included as part of the weighted sum. For the odd numbered filters an additional velocity image was produced for the central image since the central image is not included in the weighted sum for these filters.

The r.m.s. difference between each filtered image and its central image is plotted as a function of filter length in Figure 6. The errors due to the p-modes, as determined in Section 3, are also plotted in Figure 6 where it is assumed that the original p-mode signal has a 300 m s^{-1} r.m.s. amplitude. The rotation induced errors jump immediately to a level of about 1 m s^{-1} and then rise slowly to about 2 m s^{-1} after 30 min. This slow increase in the error signal is due to the smaller relative weights given to the images at

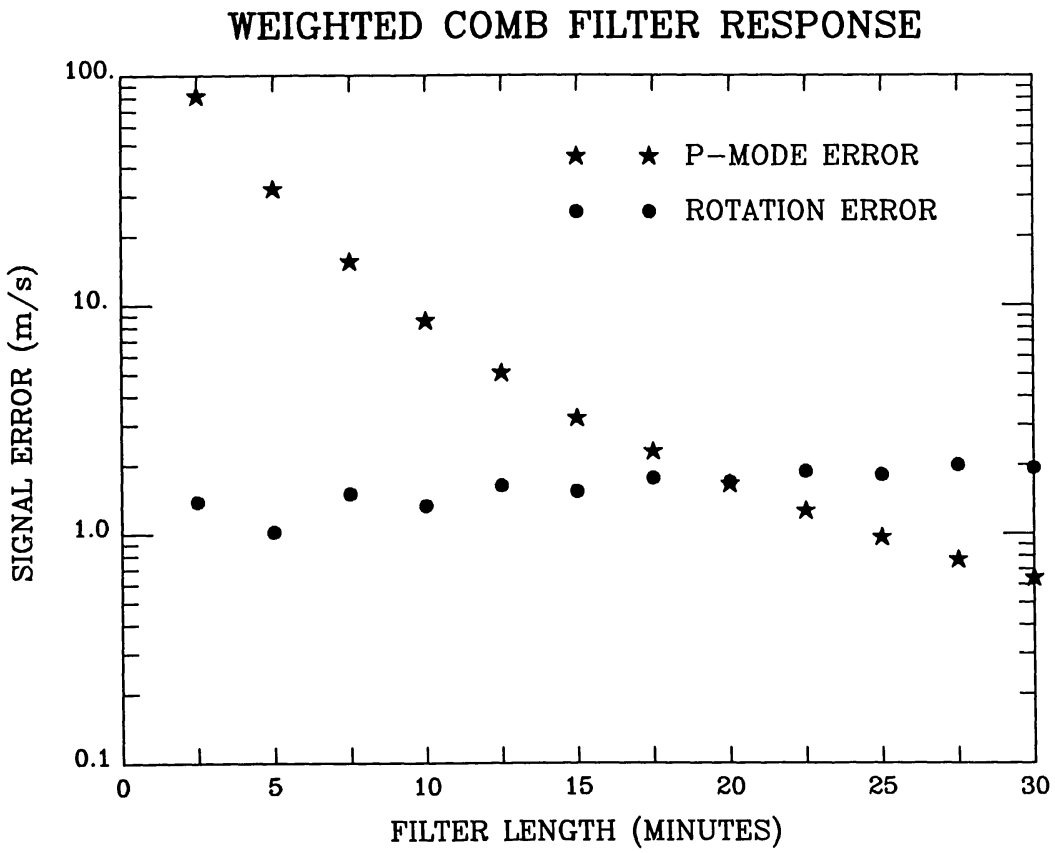

Fig. 6. The response of the weighted comb filter to the p-mode time series and to the rotation of the supergranule pattern are plotted as functions of filter length. The errors induced by solar rotation increase slowly as the filter length increases because the relative weights of the data at the extreme ends of the filtered interval become smaller. The two curves cross after about 20 min with errors at the 1.5 m s^{-1} level. Shorter filters have much larger errors from the p-modes; longer filters have slightly larger errors from the rotation of the supergranule pattern.

the extreme ends of the filtered image string. Even for the 30 min filter more than 60% of the filter weight is in the three central images which are separated by only 5 min. The odd numbered filters (those at 2.5, 7.5 min, etc.) have slightly larger error levels than the even filters (those at 5, 10 min, etc.). This is probably due to the fact that the central comparison image is not included in the weighted sum that constitutes the odd numbered filters.

The response of the weighted comb filter, as shown in Figure 6, can be used to choose an optimum filter length in which the velocity errors are minimized. The rotation-induced errors remain at a nearly constant 1 to 2 m s^{-1} while the errors due to the *p*-modes decrease rapidly from about 80 m s^{-1} for a 2.5 min filter to about 0.6 m s^{-1} for a 30 min filter. The error levels are nearly equal for filters about 20 min long with contributions from both sources of error at the 1.5 m s^{-1} level. Filters shorter than this will have much larger errors due to the *p*-modes. Filters longer than this will have slightly larger errors due to the rotation of the supergranule pattern. Although longer filters may have the added advantage of reducing random errors associated with the acquisition of the Doppler images, they also require additional time to compute.

5. Conclusions

Realistic artificial data were constructed to test various temporal filters designed to isolate the nearly steady flows in Doppler velocity data. Short filters are ineffective in suppressing the velocity signal due to the *p*-modes. Long filters introduce additional errors due to the rotation of the supergranulation pattern across the solar disk. These effects are particularly severe for simple boxcar averages but can be minimized with weighted comb filters which use data separated by 120 to 150 s so that the *p*-modes are sampled at opposite phases. The low relative weight for the data at the extreme ends of the weighted filter range helps to reduce the errors associated with the rotation of the supergranules.

The optimum filters are 20 min long weighted comb filters with data sampled at 120 or 150 s intervals. With them, the velocity errors due to both the *p*-mode signal and the rotation of the supergranules are kept at a level of about 1.5 m s^{-1}. Although these filters are considered optimal in the sense that the combined errors due to these two sources are minimized, somewhat longer filters of the same type may have added advantages. The errors due to the rotation of the supergranules increase quite slowly for longer filters while the errors due to the *p*-modes decrease rapidly. Since the pattern associated with the *p*-mode signal is distinctly different from the steady flow velocity pattern (the *p*-mode signal is strongest near disk center while the steady flow signal is strongest near the limb), it may be desirable to reduce the *p*-mode signal even further by using a somewhat longer filter. Longer filters will also help to reduce the random errors associated with the acquisition of the Doppler velocity images.

Doppler velocity images produced with these weighted comb filters will allow for precise measurements to be made of the steady flow velocity components in the solar photosphere. Some of these velocity components, in particular the meridional circu-

lation and giant cell convection, are very weak and may be evident only after filtering the data with these temporal filters. The filtered images can also be subtracted from the original data string to give data free of the steady flow components in studies of the *p*-mode oscillations themselves. There already exist several data sets associated with helioseismology observations which could be filtered in this manner. Observations with the GONG instruments and the Solar Oscillations Imager on the proposed ESA/NASA SOHO spacecraft should also provide excellent data. Analysis of the filtered data should provide an opportunity for accurately determining the nature of the photospheric velocity fields.

Acknowledgements

Support for this research was provided by the NASA Office of Solar Physics. The author is grateful for many useful discussions with colleagues in the Solar Science Branch at MSFC and members of the GONG Project, in particular John Leibacher and Jack Harvey at NSO and Hirokazu Yoshimura visiting MSFC from the University of Tokyo. He would also like to thank Allen Gary and Tauna Moorehead for their careful reading and useful comments on the manuscript as well as Ed Reichmann and James Smith for their assistance with the graphics.

References

Duvall, T. L., Jr., Harvey, J. W., Libbrecht, K. G., Popp, B. D., and Pomerantz, M. A.: 1988, *Astrophys. J.* **324**, 1158.

Grec, G., Fossat, E., and Pomerantz, M. A.: 1983, *Solar Phys.* **82**, 55.

Harvey, J. W. and Duvall, T. L., Jr.: 1984, in M. Gabriel and A. Noels (eds.), *Theoretical Problems in Stellar Stability and Oscillations*, Institut d'Astrophysique, Liège, p. 209.

Hathaway, D. H.: 1988, *Solar Phys.* (submitted).

Leibacher, J. W.: 1987, private communication.

Leighton, R. B., Noyes, R. W., and Simon, G. W.: 1962, *Astrophys. J.* **135**, 474.

Libbrecht, K. G. and Zirin, H.: 1986, *Astrophys. J.* **308**, 413.